PHYSICAL REVIEW A **86**, 031805(R) (2012)

# Pseudospin and nonlinear conical diffraction in Lieb lattices

Daniel Leykam,[1] Omri Bahat-Treidel,[1,2] and Anton S. Desyatnikov[1]
[1]*Nonlinear Physics Centre, Research School of Physics and Engineering, The Australian National University, Canberra ACT 0200, Australia*
[2]*School of Mathematics and Physics, The University of Queensland, Brisbane, Queensland 4072, Australia*
(Received 4 July 2012; published 24 September 2012)

We study linear and nonlinear wave dynamics in the Lieb lattice, in the vicinity of an intersection point between two conical bands and a flat band. We define a pseudospin operator and derive a nonlinear equation for spin-1 waves, analogous to the spin-1/2 nonlinear Dirac equation. We then study the dynamics of wave packets that are associated with different pseudospin states, and find that they are distinguished by their linear and nonlinear conical diffraction patterns.

DOI: 10.1103/PhysRevA.86.031805 PACS number(s): 42.25.Fx, 42.65.Hw

Lattices with two or more intersecting bands display fascinating phenomena such as Klein tunneling [1], pseudodiffusive transmission [2], and conical diffraction [3]. These unusual effects appear as the result of strong modification of the dispersion near the band intersection points, referred to as singular or diabolical points. One of the hallmarks of diabolical points with linear dispersion is conical diffraction, i.e., the evolution of a wave packet into a ring transverse structure with vanishing amplitude in the center [3,4]. There has been considerable recent interest in honeycomb lattices because in the vicinity of its diabolical points the wave propagation is described by a massless Dirac equation [5,6]. However, honeycomb lattices are just one example of a more general family of lattices with a singular band structure which are now being actively explored [7,8].

As opposed to the honeycomb lattice, the Lieb lattice [9], which consists of three square sublattices, displays a triply degenerate diabolical point at which two conical bands and a flat band intersect. In addition, the Lieb lattice has only one diabolical point in the first Brillouin zone (BZ), implying that the Berry phase associated with it is trivial [10]. Nevertheless, the proximity of intersecting bands with a diabolical point leads to a variety of interesting effects, which can be realized using cold atoms in optical lattices [11]. For example, when spin-orbit coupling is included, the conical bands support topologically protected edge states, while the flat band remains topologically trivial [12].

In this Rapid Communication we consider a photonic realization of the Lieb lattice and study wave dynamics near the diabolical point in the presence of Kerr nonlinearity. We define a pseudospin operator and study the evolution of wave packets associated with different pseudospin eigenstates [13]. As a specific example, we focus on conical diffraction, and demonstrate that the pseudospin degree of freedom is accessible experimentally and has real physical significance. In addition, we derive a nonlinear effective field equation for spin-1 waves and use it to study the effect of nonlinearity on wave dynamics.

We compare the dynamics predicted by our effective field equation with numerical solutions of the full nonlinear Schrödinger equation and find remarkable agreement. In particular, the conical diffraction pattern of the different spin states is different even when the nonlinearity is absent: For spin 0 the conical diffraction closely resembles the pattern obtained in honeycomb lattices [3,14]; in contrast, the spin-1 states present conical diffraction with an additional nondiffracting central spot. In the nonlinear case, the diffracting rings transform into squares, and reversing the sign of the nonlinearity changes their orientation. Our results demonstrate that the underlying pseudospin states are not merely a mathematical formality but have a physical effect which can be observed in experiments with light in photonic lattices and with Bose-Einstein condensates trapped in optical lattices [11].

The propagation equation for a monochromatic field envelope $\psi$ in a two-dimensional photonic lattice is

$$i\partial_z\psi = \hat{H}_0\psi + g|\psi|^2\psi, \quad \hat{H}_0 = -\nabla_\perp^2 - V(\mathbf{r}_\perp), \qquad (1)$$

where $V(\mathbf{r}_\perp)$ is the periodic refractive index and $g = \mp 1$ accounts for defocusing or focusing Kerr nonlinearity. The Lieb lattice refractive index is shown in Fig. 1(a).

It is instructive to study the linear ($g = 0$) regime first; it will lead us to show that the system incorporates a pseudospin, which corresponds to an actual degree of freedom and affects the nonlinear dynamics. Understanding the pseudospin structure of a system can explain very exotic phenomena such as weak antilocalization in graphene [15] and nonlinear Klein tunneling [16].

The Lieb lattice has three sites in each unit cell denoted by $A$, $B$, and $C$ in Fig. 1(a). It is convenient to write the Hamiltonian $\hat{H}_0$ in a tight-binding form,

$$\hat{H}_0 = \sum_{\boldsymbol{R}_n,\boldsymbol{\delta}_j} [t(a_n^\dagger b_n + b_n^\dagger c_n) + t' a_n^\dagger c_n + \text{H.c.}], \qquad (2)$$

where $a_n, b_n, c_n$ are the annihilation operators associated with functions localized around the $A, B, C$ sites (e.g., Wannier states [17]) in the $n$th unit cell, $\boldsymbol{R}_n$ is the position of the unit cell, and $\boldsymbol{\delta}_j$ are the vectors connecting the neighbors with the hopping parameters (coupling coefficients) $t$ and $t'$ [see Fig. 1(a)]. Transforming to momentum space and defining $\Phi_{\boldsymbol{k}}^\dagger = (a_{\boldsymbol{k}}^\dagger\ b_{\boldsymbol{k}}^\dagger\ c_{\boldsymbol{k}}^\dagger)$, Eq. (2) becomes $\hat{H}_0 = \sum_{\boldsymbol{k}} \Phi_{\boldsymbol{k}}^\dagger \mathcal{H}_{\boldsymbol{k}} \Phi_{\boldsymbol{k}}$, where

$$\mathcal{H}_{\boldsymbol{k}} = 2t \begin{bmatrix} 0 & \cos k_x & 2\gamma \cos k_x \cos k_y \\ \cos k_x & 0 & \cos k_y \\ 2\gamma \cos k_x \cos k_y & \cos k_y & 0 \end{bmatrix}, \qquad (3)$$

$\gamma = t'/t$, and $-\pi/2 \leqslant k_{x,y} \leqslant \pi/2$. In the absence of NNN coupling ($\gamma = 0$) the spectrum is

$$\beta(\boldsymbol{k}) = 0, \pm 2t\eta(\boldsymbol{k}), \quad \eta(\boldsymbol{k}) \equiv \sqrt{\cos^2 k_x + \cos^2 k_y}, \qquad (4)$$

 

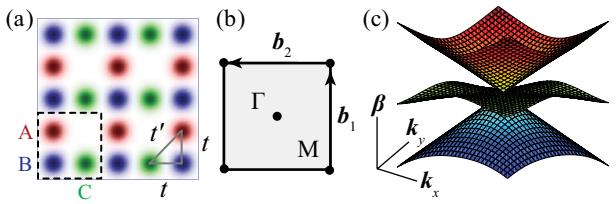


FIG. 1. (Color online) (a) The lattice potential, with three sites per unit cell (dashed square). The sublattices are marked A (red), B (blue), and C (green). The nearest-neighbor (NN) and next-to-nearest-neighbor (NNN) coupling are shown as $t$ and $t'$. (b) First Brillouin zone. (c) First three bands in the vicinity of the $M$ point.

with the corresponding eigenstates

$$\psi_0 = (-\cos k_y \quad 0 \quad \cos k_x), \tag{5}$$

$$\psi_\pm = (2\eta)^{-1/2}[\cos k_x \quad \pm\eta(\boldsymbol{k}) \quad \cos k_y]. \tag{6}$$

We refer to the $\beta(\boldsymbol{k}) = 0$ as the flat band, and the other two branches as conical bands. Note that for each state $|\beta,\boldsymbol{k}\rangle$ there is a corresponding state $|-\beta,\boldsymbol{k}\rangle$. This symmetry, which is known as particle-hole symmetry, exists whenever there is some operator $\hat{O}$ that anticommutes with the Hamiltonian, in this case $\hat{O} = \mathrm{diag}(1,-1,1)$. The symmetry is broken by the NNN term ($\gamma \neq 0$).

The three bands intersect at the $M$ point, $\boldsymbol{k}_M = (\frac{\pi}{2},\frac{\pi}{2})$ [see Figs. 1(b) and 1(c)]. Expanding $\mathcal{H}_{\boldsymbol{k}}$ around the intersection point and denoting by $\boldsymbol{p}$ the displacement from the $M$ point, we obtain

$$\mathcal{H}_{\boldsymbol{p}} = 2t \begin{bmatrix} 0 & p_x + \frac{p_x^3}{24} & 2\gamma p_x p_y \\ p_x + \frac{p_x^3}{24} & 0 & p_y + \frac{p_y^3}{24} \\ 2\gamma p_x p_y & p_y + \frac{p_y^3}{24} & 0 \end{bmatrix}. \tag{7}$$

In the absence of NNN coupling ($\gamma = 0$), to leading order the spectrum is isotropic, $\beta = 0, \pm 2t|\boldsymbol{p}|$, and the angular momentum (AM) should be a constant of motion. However, the orbital AM $L_z$ is not conserved, $d\hat{L}_z/dt \propto [\mathcal{H}_{\boldsymbol{p}},\hat{L}_z] \neq 0$, suggesting that there is some additional AM in the system which may restore the conservation of the total AM. As was shown in the Ref. [18], the sublattice degree of freedom in honeycomb lattices, usually referred to as pseudospin, carries the missing AM. Here we show that in the Lieb lattice the "missing" pseudospin part of the total AM can be also introduced, however, it cannot be identified with the sublattice. We define the pseudospin $\hat{S}_z$ according to the requirement that the total AM is conserved, $[\mathcal{H}_{\boldsymbol{p}},\hat{L}_z + \hat{S}_z] = 0$, and find

$$S_z = \begin{bmatrix} 0 & 0 & -i \\ 0 & 0 & 0 \\ i & 0 & 0 \end{bmatrix}, \quad S_x = \begin{bmatrix} 0 & 1 & 0 \\ 1 & 0 & 0 \\ 0 & 0 & 0 \end{bmatrix},$$

$$S_y = \begin{bmatrix} 0 & 0 & 0 \\ 0 & 0 & 1 \\ 0 & 1 & 0 \end{bmatrix}, \tag{8}$$

corresponding to spin 1. The matrices $S_x, S_y$ are defined to satisfy the usual AM algebra, $[S_i,S_j] = i\epsilon_{ijk}S_k$, for later notational convenience. We emphasize that the spin matrices are written in the sublattice basis, and that $S_z$ is not diagonal, meaning that the pseudospin and the sublattice cannot be associated with each other as in the case of honeycomb lattices. Writing the eigenstates of $S_z$ in the sublattice basis illustrates how to construct these states in experiments. Diagonalizing $S_z$ we find

$$v_0^T = (0 \quad 1 \quad 0), \quad v_{\pm 1}^T = \frac{1}{\sqrt{2}}(\pm i \quad 0 \quad 1), \tag{9}$$

meaning that the $|S_z = 0\rangle$ state has vanishing amplitude on the $A$ and $C$ sublattices, whereas the $|S_z = \pm 1\rangle$ states have vanishing amplitude on the $B$ sublattice and a relative phase of $\pi/2$ between the $A$ and $C$ sublattices. In the following we show the physical significance of the pseudospin by studying the nonlinear conical diffraction of the different pseudospin states.

To include Kerr nonlinearity we use the effective-mass approximation [17] and derive the effective Hamiltonian in real space. The wave-packet envelopes corresponding to the three sublattices are conveniently written as a three-component spinor $\Psi^T = (\Psi_a \ \Psi_b \ \Psi_c)$. Since the nonlinearity is local, it is diagonal in the sublattice basis [16], resulting in

$$i\partial_z\Psi = [\widetilde{\mathcal{H}}\{i\partial_j\} + g\hat{n}]\Psi, \tag{10}$$

where $\widetilde{\mathcal{H}}\{i\partial_j\}$ is $\mathcal{H}_{\boldsymbol{p}}$ with the replacement $p_j \to i\partial_j$, and $\hat{n} = \mathrm{diag}(|\Psi_a|^2,|\Psi_b|^2,|\Psi_c|^2)$. This equation is derived in a similar manner to the nonlinear Dirac equation in honeycomb lattices [19,20]. As was shown in Ref. [21], the nonlinearity drives the waves out of the vicinity of the conical intersection. This is taken into account by including the higher-order terms in the momentum expansion [16,22]. We emphasize that this nonlinear equation is very unique, and it takes a simple form when the high-order terms can be neglected,

$$i\partial_z\Psi = [2it\boldsymbol{S}_\perp \cdot \boldsymbol{\nabla}_\perp + V_{\mathrm{ex}}(\boldsymbol{r}) + g\hat{n}]\Psi, \tag{11}$$

which is a spin-1 variation of the massless nonlinear Dirac equation, where we have included an additional external potential that varies slowly of a scale of a lattice constant.

We study the nonlinear wave-packet dynamics of the different pseudospin states by solving both the effective Eq. (10) and the nonlinear Schrödinger Eq. (1), and making a quantitative comparison between them. An important tool for the analysis and understanding of the dynamics is a Bloch distribution analysis presented in detail in Ref. [21]. The spectrum in Fig. 1(c) is obtained numerically along with the eigenstates of $H_0$ and the Bloch modes $\mathcal{B}_{n,\boldsymbol{k}}$. The projections of the wave function onto the Bloch modes $\langle\mathcal{B}_{n,\boldsymbol{k}}|\psi\rangle$ are calculated to obtain the total population in the $n$th band, $P_n = \sum_{\boldsymbol{k}} |\langle\mathcal{B}_{n,\boldsymbol{k}}|\psi\rangle|^2$. This tells us how the nonlinearity redistributes the population between the different bands, which causes very different dynamics. For example, the flat-band population does not diffract at all whereas the conical bands have very strong diffraction. We find good quantitative agreement between the populations calculated from the effective model and the solution of Eq. (1).

The input beams corresponding to different pseudospin eigenstates are constructed by selectively exciting the different sublattices, as in Fig. 2(a), with a plane-wave envelope corresponding to the $M$ point. In all cases, the total projection onto the first three bands is over 98%, indicating that our three-band approximation is well justified. In experiments these inputs could be approximated by interfering tilted broad

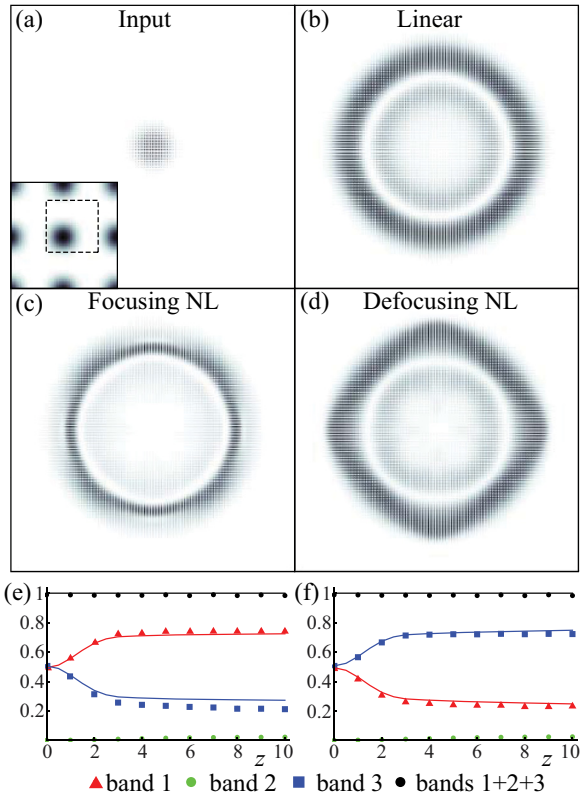


FIG. 2. (Color online) (a) Pseudospin-0 input Gaussian beam at the $M$ point. (b) Linear output; the inset shows a greatly magnified part of the beam with one sublattice excited in the (dashed) unit cell. (c), (d) Outputs with focusing and defocusing nonlinearities, with the input beam power 81.6. (e), (f) Bloch band populations as a function of $z$ for focusing and defocusing nonlinearities. Markers are obtained by solving Eq. (1) while curves are obtained from the effective model Eq. (10).

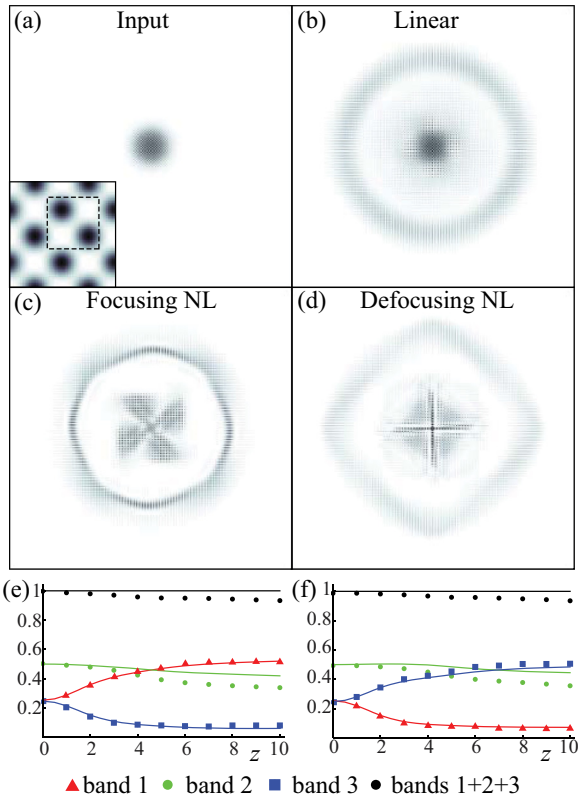


FIG. 3. (Color online) (a) Pseudospin-1 input beam at the $M$ point. Similar to Fig. 2, here (b) shows the linear output, (c), (d) the outputs with focusing and defocusing nonlinearities for input power 162.3, and (e), (f) corresponding Bloch band populations as a function of $z$.

Gaussian beams positioned at the four corners of the BZ, with different relative phases controlling the spin: Equal phases at four corners corresponds to $S_z = 0$, while $S_z = \pm 1$ is obtained with a phase difference of $\pm\pi/2$ between adjacent corners of the BZ. The dimensionless parameters used in the numerical solution of Eq. (1) are $\max(V) = 25$, $\max(z) = 20$, and a lattice period of 2.

For the pseudospin-0 eigenstate $|S_z = 0\rangle = (0\ 1\ 0)$, corresponding to the $B$ sublattice, we find that in the low-intensity limit ($g = 0$) the input beam in Fig. 2(a) evolves into two circular bright rings of constant width in Fig. 2(b), which is characteristic of conical diffraction [3]. When nonlinearity is introduced, there is a redistribution of the Bloch modes comprising the wave packet, and the resulting diffraction pattern has the symmetry of the energy manifold $\beta(\boldsymbol{k})$ around the diabolic point [21]. The diffraction of the lower conical band population is rotated by $\pi$, since its propagation angle (analogous to group velocity) $\nabla_k \beta(\boldsymbol{k})$ is opposite. In our case, the energy manifold has fourfold symmetry, and therefore the sign of the nonlinearity should not affect the diffraction pattern. Surprisingly, the numerical solution of Eq. (1) presents a different picture: Indeed, both focusing and defocusing nonlinear cases present the expected fourfold symmetry of the deformed rings, but the two cases are rotated by $\pi/4$ with respect to each other; cf. Figs. 2(c) and 2(d). To explain this, we solve the effective model, Eq. (10), without NNN coupling ($\gamma = 0$), and find that the two diffraction patterns are not rotated with respect to each other, and when the NNN coupling is introduced ($\gamma \neq 0$), the $\pi/4$ rotation is reproduced. Therefore, in the nonlinear dynamics in the Lieb lattice, the NNN coupling has a major qualitative effect, in contrast to honeycomb lattices. In addition, the Bloch analysis reveals a very interesting fact: The flat band which is initially empty (since $\langle\psi_0|S_z = 0\rangle = 0$) remains nearly empty during the propagation even though the nonlinearity has a significant effect on the band populations; cf. Figs. 2(e) and 2(f). This means that there is a selection rule in the process of four-wave mixing.

This selection rule can be understood by using an approximation of a thin-layer nonlinear medium, which is justified for sufficiently weak nonlinearity (low input power): The input beam diffracts rapidly, the amplitude decays, and the nonlinear term only acts for a short distance. In this regime, the population transfer between the bands $\alpha$ and $\beta$ is proportional to $\langle\psi_\alpha|\hat{n}(0)|\psi_\beta\rangle$. For an initial state $|S_z = 0\rangle \leftrightarrow (0\ \Psi_b\ 0)$, the matrix element $\langle\psi_0|\hat{n}(0)|\psi_\pm\rangle$ vanishes [23], and therefore there is no population transfer between the conical bands and the flat band, which is exactly the selection rule found in the numerical calculations. Moreover, one can write the nonlinear term $\hat{n}$ in the pseudospin basis and see that the $S_z = 0$ subspace is decoupled, i.e., the nonlinearity does not mix the $S_z = 0$ state with the $S_z = \pm 1$ states.

For the pseudospin-1 states $|S_z = \pm 1\rangle = 1/\sqrt{2}(\pm i\ 0\ 1)$, which have a vanishing amplitude on the $B$ sublattice [Fig. 3(a)], we find even greater differences. In the linear case the evolution of the input beam [Fig. 3(a)] into a conical pattern is accompanied by a very bright central spot [Fig. 3(b)]. By calculating the projections of the wave packet of the Bloch modes of the various bands, we find that the spin-$\pm 1$ states carry about 50% of the population in the flat band. During the initial nonlinear propagation part of it, $\sim$10%, is transferred to the conical bands. The modes of the flat band have vanishing group velocity, corresponding to nondiffracting beams, which is why the central spot does not diffract, and the nonlinearity has a greater effect. Here we have doubled the input beam power (with respect to Fig. 2) so that the power initially residing in the conical bands is identical to the pseudospin-0 case. Consequently, the structure of the square-deformed diffracting rings [Figs. 3(c) and 3(d)] is very similar. In addition, the central spot has a chiral pattern which is reversed for the opposite spin states $\pm 1$ with the same nonlinearity (not shown); this effect can be used to distinguish the $\pm 1$ states. Therefore, in the presence of nonlinearity the medium is effectively chiral, as it affects wave packets with different AM differently.

In conclusion, we have studied nonlinear wave dynamics in Lieb lattices, and have shown that it is strongly dependent on the pseudospin. In addition, we derived a spin-1 nonlinear wave equation resembling the nonlinear Dirac equation. We have demonstrated experimental accessibility of the pseudospin via conical diffraction which is qualitatively different from the honeycomb lattice case. Some of the differences result from the fact that in the honeycomb lattices the pseudospin 1/2 can be identified with the sublattice, whereas in Lieb lattices there is a clear distinction between the two. Other differences originate from the band structure and the existence of the flat band. It would be intriguing to study similar dynamics in the kagome lattice [24], which was recently realized experimentally [25]. The latter is also a tripartite lattice, presumably with pseudospin 1, but it has the same underlying symmetries as the honeycomb lattice.

This work is supported by the Australian Research Council.

[1] M. I. Katsnelson, K. S. Novoselov, and A. K. Geim, Nat. Phys. **2**, 620 (2006).
[2] R. A. Sepkhanov, Y. B. Bazaliy, and C. W. J. Beenakker, Phys. Rev. A **75**, 063813 (2007).
[3] O. Peleg, G. Bartal, B. Freedman, O. Manela, M. Segev, and D. N. Christodoulides, Phys. Rev. Lett. **98**, 103901 (2007).
[4] M. V. Berry and M. R. Jeffrey, Prog. Opt. **50**, 13 (2007).
[5] D. P. DiVincenzo and E. J. Mele, Phys. Rev. Lett. **53**, 52 (1984).
[6] G. W. Semenoff, Phys. Rev. Lett. **53**, 2449 (1984).
[7] K. Asano and C. Hotta, Phys. Rev. B **83**, 245125 (2011).
[8] B. Dóra, J. Kailasvuori, and R. Moessner, Phys. Rev. B **84**, 195422 (2011).
[9] E. H. Lieb, Phys. Rev. Lett. **62**, 1201 (1989).
[10] R. Shen, L. B. Shao, B. Wang, and D. Y. Xing, Phys. Rev. B **81**, 041410 (2010).
[11] V. Apaja, M. Hyrkäs, and M. Manninen, Phys. Rev. A **82**, 041402 (2010).
[12] C. Weeks and M. Franz, Phys. Rev. B **82**, 085310 (2010).
[13] N. Goldman, D. F. Urban, and D. Bercioux, Phys. Rev. A **83**, 063601 (2011).
[14] O. Bahat-Treidel, O. Peleg, and M. Segev, Opt. Lett. **33**, 2251 (2008).
[15] H. Suzuura and T. Ando, Phys. Rev. Lett. **89**, 266603 (2002).
[16] O. Bahat-Treidel and M. Segev, Phys. Rev. A **84**, 021802 (2011).
[17] C. Kittel, *Quantum Theory of Solids* (Wiley, New York, 1963).
[18] M. Mecklenburg and B. C. Regan, Phys. Rev. Lett. **106**, 116803 (2011).
[19] M. J. Ablowitz, S. D. Nixon, and Y. Zhu, Phys. Rev. A **79**, 053830 (2009).
[20] L. D. Haddad and L. H. Carr, Physica D **238**, 1413 (2009).
[21] O. Bahat-Treidel, O. Peleg, M. Segev, and H. Buljan, Phys. Rev. A **82**, 013830 (2010).
[22] M. J. Ablowitz and Y. Zhu, Opt. Lett. **36**, 3762 (2011).
[23] This statement holds when the Hamiltonian eigenstates calculated in the presence of the NNN coupling are included as well.
[24] I. Syôzi, Prog. Theor. Phys. **6**, 306 (1951).
[25] M. Boguslawski, P. Rose, and C. Denz, Appl. Phys. Lett. **98**, 061111 (2011).